Deep Learning at Scale for Gravitational Wave Parameter Estimation of Binary Black Hole Mergers

Hongyu Shen,^{1,2} E. A. Huerta,^{1,3} and Zhizhen Zhao^{1,2,4}

¹NCSA, University of Illinois at Urbana-Champaign, Urbana, Illinois 61801, USA

²Department of Electrical and Computer Engineering, University of Illinois at Urbana-Champaign, Urbana, Illinois 61801, USA

³Department of Astronomy, University of Illinois at Urbana-Champaign, Urbana, Illinois 61801, USA

⁴Coordinated Science Laboratory, University of Illinois at Urbana-Champaign, Urbana, Illinois 61801, USA

(Dated: April 5, 2022)

We present the first application of deep learning at scale to do gravitational wave parameter estimation of binary black hole mergers that describe a 4-D signal manifold, i.e., black holes whose spins are aligned or anti-aligned, and which evolve on quasi-circular orbits. We densely sample this 4-D signal manifold using over three hundred thousand simulated waveforms. In order to cover a broad range of astrophysically motivated scenarios, we synthetically enhance this waveform dataset to ensure that our deep learning algorithms can process waveforms located at any point in the data stream of gravitational wave detectors (time invariance) for a broad range of signal-to-noise ratios (scale invariance), which in turn means that our neural network models are trained with over 10⁷ waveform signals. We then apply these neural network models to estimate the astrophysical parameters of black hole mergers, and their corresponding black hole remnants, including the final spin and the gravitational wave quasi-normal frequencies. These neural network models represent the first time deep learning is used to provide point-parameter estimation calculations endowed with statistical errors. For each binary black hole merger that ground-based gravitational wave detectors have observed, our deep learning algorithms can reconstruct its parameters within 2 milliseconds using a single Tesla V100 GPU. We show that this new approach produces parameter estimation results that are consistent with Bayesian analyses that have been used to reconstruct the parameters of the catalog of binary black hole mergers observed by the advanced LIGO and Virgo detectors.

I. INTRODUCTION

Gravitational wave (GW) sources [1–6] are now routinely detected by the advanced LIGO [7, 8] and Virgo [9] detectors. The last two observing runs of these GW detectors indicate that, on average, one GW source has been detected for every fifteen days of analyzed data. It is expected that this number will be superseded in the upcoming third observing run, since the advanced LIGO and Virgo detectors have been undergoing commissioning since August 2017. In their enhanced volumetric configuration, it is expected that the detection rate for binary black hole (BBH) mergers and binary neutron star (BNS) inspirals will increase, and may yield the first observations of neutron star-black hole (NSBH) mergers [6].

Given the expected scale of GW discovery in upcoming observing runs, it is in order to explore the use of efficient signal-processing algorithms for low-latency GW detection and parameter estimation. This work is motivated by the need to probe a deeper parameter space that is available to GW detectors, in real-time, and using minimal computational resources to maximize the number of studies that can be conducted with GW data. This combination of constraints is a common theme for large-scale astronomical facilities, which will be producing large datasets in low-latency within the next decade, e.g., the Large Synoptic Survey Telescope [10]. Scenarios in which both LSST, among other electromagnetic observatories, and advanced LIGO and Virgo work in unison, analyzing disparate datasets in real-time to realize the science goals of Multi-Messenger Astrophysics make this work timely and relevant [11, 12].

Among a number of recent developments in signalprocessing, deep learning exhibits great promise to increase the speed and depth of real-time GW searches. The first deep learning algorithms to do classification and regression of GWs emitted by non-spinning BBHs on quasi-circular orbits were presented in [13] in the context of simulated LIGO noise. The extension of that study to realistic detection scenarios using real advanced LIGO noise was introduced in [14]. Even though these algorithms were trained to do real-time classification and regression of GWs in realistic detection scenarios for a 2-D signal manifold (non-spinning BBHs on quasi-circular orbits), the studies presented in [13–15] have demonstrated that deep learning algorithms generalize to new types of sources, enabling the identification of moderately eccentric BBH mergers, spin precessing BBH mergers, and moderately eccentric BBH signals that include higher-order modes, respectively. These studies also indicate that while the detection of these new types of GW sources is possible, it is necessary to use higherdimensional signal manifolds to train these algorithms to improve parameter estimation results, and to go beyond point-parameter estimation analysis. This work has sparked the interest of the GW community, leading to a variety of studies including the classification of simulated BBH waveforms in Gaussian noise, GW source modeling and GW denoising of BBH mergers [15–27].

While detection and parameter estimation are the key goals for the development of deep learning for GW astrophysics, in this article we focus on the application of deep learning for parameter estimation. At present, GW parameter estimation is done using Bayesian inference [28, 29], which is a robust, yet computationally-intensive approach. Given the scalability and robustness of deep learning algorithms, it is natural to explore their applicability for GW parameter estimation, the theme of this article.

Previous Work The first exploration of deep learning for a 2-D signal manifold was presented in [13, 14]. For waveform signals with matched-filtering signal-to-noise ratio (SNR) SNR $\gtrsim 10$, these neural network models measure the masses of quasi-circular BBH mergers with a mean percentage absolute error $\lesssim 15\%$, and with errors $\lesssim 35\%$ for moderately eccentric BBH mergers. These results provided a glimpse of the robustness and scalability of deep neural network models, and the motivation to take these prototypical applications into a production run toolkit for GW parameter estimation.

Highlights of This Work We have designed new architectures and training schemes to demonstrate that deep learning provides the means to reconstruct the parameters of BBH mergers in more realistic astrophysical settings, i.e., black holes whose spins are aligned or antialigned, and which evolve on quasi-circular orbits. This 4-D signal manifold marks the first time deep learning at scale is used for GW data analysis, since we have utilized nearly 10 million waveforms to train neural network models that, once fully trained, can reconstruct in real-time the parameters of the BBH catalog presented by the LIGO and Virgo Scientific Collaborations in [6]. The neural network models we introduce in this article have two different architectures. The first one is tailored for the measurement of the masses of the binary components, whereas the second is used to quantify the final spin and the quasi-normal modes (QNMs) of the BH remnant. Once both neural networks are fully trained, we use them in parallel for inferences studies, finding that we can reconstruct the parameters of BBH mergers within 2 milliseconds using a single Tesla V100 GPU. We also show that by measuring these parameters we can infer the individual spins of the binary components that best reproduce the observed BBH signals in real LIGO noise, providing an alternative approach to better constrain the highly degenerate spin parameter space of BBH signals.

This article is structured as follows. Section II introduces the model architectures used in these analyses, it describes the construction and curation of the datasets used to train, validate and test our neural network models. It also includes a revised curriculum learning for neural network training. We quantify the accuracy of these neural network models in realistic detection scenarios using real advanced LIGO noise in Section III. We put at work our deep learning algorithms in Section IV to estimate the astrophysical parameters of the BBH mergers reported in [6]. We summarize our findings and future directions of work in Section V.

II. METHODS

In this section, we introduce the neural network models used for parameter estimation, and describe a novel curriculum learning scheme to accurately measure the masses of the binary components, and the final spin and QNMs of the BH remnant. We have used TensorFlow [30, 31] to design, train, validate and test the neural network models presented in this section.

The rationale to use two neural network models stems from the fact that the masses, spins and QNMs span rather different scales. Therefore, to improve the accuracy with which deep learning can measure these parameters we have designed one neural network that is tailored to measure the masses of the binary components, and one to measure the final spin and QNMs of the remnant. The astute reader may have noticed that the final spin of the BH remnant and its QNMs have a similar range of values when the QNMs are cast in dimensionless units, and this is the approach we have followed. In practice, we train the second neural network model using the fact that the QNMs are determined by the final spin a_f using the relation [32]

$$\omega_{220} \left(a_f \right) = \omega_R + i \, \omega_I \,, \tag{1}$$

where (ω_R, ω_I) correspond to the frequency and damping time of the ringdown oscillations for the fundamental $\ell=m=2$ bar mode, and the first overtone n=0. We have computed the QNMs following [32]. One can readily translate ω_R into the ringdown frequency (in units of Hertz) and ω_I into the corresponding (inverse) damping time (in units of seconds) by computing $M_f \omega_{220}$. M_f represents the final mass of the remnant, and can be determined using Eq. (1) in [33].

As we describe below, we have found that to accurately reconstruct the masses of the binary components, it is necessary to use a more complex and deeper neural network architecture. It is worth mentioning that once these models are fully trained, a single GPU is sufficient to perform regression analyses in milliseconds using both neural network models.

A. Neural network model to measure the properties of the black hole remnant

The neural network model consists of two main parts: a shared root component for all physical parameters, and three leaf components for individual parameters $(a_f, \omega_R,$ and $\omega_I)$, as illustrated in the left panel of Figure 1, and Table I. The model architecture looks like a rooted tree. The root is composed of seven convolutional layers, and its output is shared by the leaves. Each leaf component has the same network architecture with three fully connected layers. This approach is inspired by the hierarchical self decomposing of convolutional neural networks

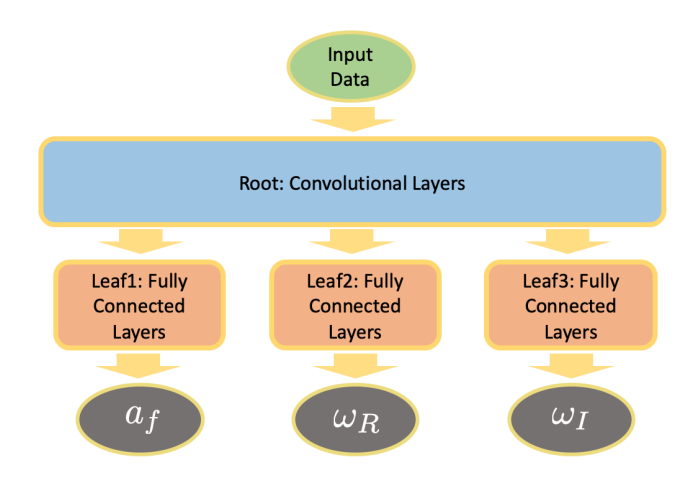


FIG. 1. Architecture of the neural network used to estimate the final mass and quasi-normal modes of the black hole remnant.

described in [34, 35]. The key idea behind this approach is that the neural network structures are composed of a general feature extractor for the first seven layers, which is then followed up by sub-networks that take values from the output of the general feature extractor.

The rationale to have splits after the universal structure is to use sub-structures that focus on different sub-groups of the data. As a simile: even though the human body has multiple limb locations ("leaves"), human motion is controlled by the overall motion of the body ("the root"). In practice this means that the tree structure of our models leverages the hierarchical structure of the data. It first extracts the universal features through the root, and then passes the information to the different sub-networks ("leaves") to learn specialized features for different physical parameters. Notice that the root will also prevent overfitting in the "leaves", since each leaf is optimized through the root.

Another change to the conventional architecture is that we remove the nonlinear activation in the second to last layer in the leaf component, i.e., it is a linear layer with identity activation function (see Table I). This allows more neurons to be activated and passed to the final layer. As discussed in [36], removing the nonlinear activation in some intermediate layers smooths the gradients and maintains the correlation of the gradients in the neural network weights, which, in turn, allows more information to be passed through the network as the depth increases.

B. Neural network model to measure the masses of the binary components

The tree-like network model used for this study is described in the right panel of Figure 2 and Table II. With

TABLE I. Architecture of the neural network model used to measure the final spin and QNMs of the black hole remnant. For the root convolutional layers, the setup indicates: (kernel size, # of output channels, stride, dilation rate, max pooling kernel, max pooling stride). All convolutional layers have ReLU activation function and the padding is set to "VALID" mode. There is no max pooling layer if the last two entries in the configuration are 0's. The leaf fully connected layers setup: (# of output neurons, dropout rate). For the last layer, we use tanh activation function. However, the activation function in the second last layer is removed.

Layer	Layer	Activation
Component	Configurations	Functions
Root Layer: Convolutional	$ \begin{array}{c} (16,64,1,1,4,4) \\ (16,128,1,2,4,4) \\ (16,256,1,2,4,4) \\ (32,256,1,2,4,4) \\ (4,128,1,2,0,0) \\ (4,128,1,2,0,0) \\ (2,64,1,1,0,0) \end{array} $	ReLU
Leaf Layer: Fully Connected	$ \begin{array}{c} (128, 0.0) \\ (128, 0.0) \\ (1, 0.0) \end{array} $	ReLU Identity Tanh

respect to the architecture described in the previous section, we reduce the number of convolutional layers in the root from seven to three. We have done this because we are now using more layers in the leaves, which in turn makes the gradient back-propagation harder. Reducing the number of root layers improves gradient updates to the front layers.

Each leaf component uses a squeeze-and-excitation (SE) structure [35]. The SE block is a sub-structure between two layers (squeeze step). It applies a global pooling, and assigns weights to each of the channels in the convolutional layers (excitation step). Compared to conventional convolutional structures with universal weights, the SE components adjust the importance of each channel with an adaptively learned weight, which, as described in [35], effectively results in 25% improvement in image classification. For images, channels are usually represented in RGB. Since we are using 1-D time-series signals, we treat channels of the original input signals to be 1. The SE block adaptively recalibrates channelwise feature responses. Furthermore, the weights are optimally learned through a constraint introduced by the global pooling. This ensures that the weights encode both spatial and channel-wise information. Furthermore, the weights help the channels represent group specific features at deeper layers, which is consistent with our objective of using "leaves" for different parameters.

Following the SE components, the neural networks have two highway blocks [37]. The structures are a variant of the residual structure, as proposed in [38]. In the residual block, instead of directly learning the feature, it learns the residual components by an identity shortcut connection, which resolves the gradients vanishing when

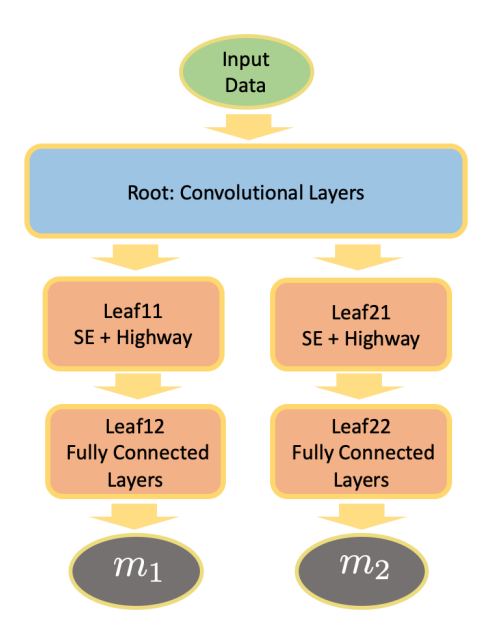


FIG. 2. Architecture of the neural network used to estimate the masses of the binary black hole components.

TABLE II. Architecture of the neural network model used to measure the masses of the binary components. For the root convolutional layers, the setup indicates: (kernel size, # of output channels, stride, dilation rate, max pooling kernel, max pooling stride). All convolutional layers have ReLU activation function and the padding is set to "VALID" mode. For the Leaf SE layer, the setup is: (# of output channels, # of residual blocks). The general structure for the SE layer follows the configuration described in [35]. Leaf highway layer setup: (kernel size, # of channels, stride, # of highway blocks). The configuration for the highway is described in [37]. The leaf fully connected layers setup is: (# of output neurons, dropout rate). For the last layer we use ReLU activation. However, the activation function in the second last layer is removed.

Layer	Layer	Activation
Component	Configurations	Functions
Root Layer: Convolutional	$ \begin{array}{c} (16,64,1,2,4,4) \\ (16,128,1,2,4,4) \\ (16,128,1,2,4,4) \end{array} $	ReLU
Leaf Layer: SE	(128,3) $(128,3)$	ReLU
Leaf Layer: Highway	(4, 128, 2, 30)	ReLU
Leaf Layer: Fully Connected	$ \begin{array}{c} (512, 0.1) \\ (256, 0.1) \\ (1, 0.0) \end{array} $	ReLU Identity ReLU

the model goes deeper. The highway block only introduces weights to the components in the residual block, which is similar to the application of importance weights on channels in SE components. Finally, we apply three fully connected layers with dropouts after the highway blocks to prevent overfitting [39]. The same nonlinearity reduction is also applied in the second last layer.

C. Dataset Preparation

To demonstrate the use of deep learning for parameter estimation, we consider the catalog of BBH mergers presented in [6]. Based on the Bayesian analyses presented in that study, we consider the following parameter space to produce our training dataset: $m_1 \in [9\mathrm{M}_\odot, 65\mathrm{M}_\odot]$, $m_2 \in [5.2\mathrm{M}_\odot, 42\mathrm{M}_\odot]$. The spin of the binary components span a range $a_{\{1,2\}} \in [-0.8, 0.8]$. By uniformly sampling this parameter space we produce a dataset with 300,180 waveforms. These waveforms are produced with the surrogate waveform family [40], considering the last second of the evolution which includes the late inspiral, merger and ringdown. The waveforms are produced using a sample rate of 8192Hz.

For training purposes, we label the waveforms using the masses and spins of the binary components, and then use this information to also enable the neural net to estimate the final spin of the BH remnant using the formulae provided in [41], and the QNMs of the ringdown following [32]. In essence, we are training our neural network models to identify the key features that determine the properties of the BBHs before and after merger using a unified framework.

In order to encapsulate the true properties of advanced LIGO noise, we whiten all the training templates using real LIGO noise from the Hanford and Livingstone detectors gathered during the first and second observing runs [42].

We use 70\% of these waveform samples for training, 15% for validation, and 15% for testing. The training samples are randomly and uniformly chosen. Throughout the training, we use ADAM optimizer to minimize the mean squared error of the predicted parameters with default hyper-parameter setups [43]. We choose the batch size to be 64, the learning rate to be 0.0008, the total number of iterations to be 120,000 (maximum). We use a dropout rate 0.1 for training and no dropout is applied for testing and validation. To simulate the environment where the true GWs are embedded, we use real advanced LIGO noise to compute power spectral density, which is then used to whiten the templates. In addition, we apply a random 0% to 6% left or right shifts. This endows the neural networks with time-invariance, and improves their performance to estimate the parameters of the signal irrespective of their position in the data stream. On the other hand, this technique also prevents overfitting of the data. Since the locations are randomly shifted with independent noise injected, the training data are different at each epoch.

D. Curriculum learning with decreasing signal-to-noise ratio

In realistic detection scenarios, GWs have moderate SNRs, and are contaminated by non-Gaussian and non-stationary noise. In order to ensure that neural networks

TABLE III. Decreasing peak SNR (pSNR) setup. The pSNR is uniformly chosen within the indicated range. Notice that the early stopping criterion is also applied if the number of iterations is greater than 60,000 and the relative error threshold is met. The relation between match-filtering SNR to pSNR is: 1.0 pSNR \approx 13.0 SNR.

Iterations	PSNRs
1-9000	2.0-3.0
9001-18000	1.5-3.0
18001-27000	1.0-3.0
27001-36000	0.5 - 3.0
36001-48000	0.3-3.0
48001-60000	0.2-3.0
60001-	0.1-3.0

identify GWs over a broad range of astrophysically motivated SNRs, we start training them with large SNRs, and gradually reduce the SNRs to a lower level. This is an idea taken from curriculum learning literature [44], which allows the network to distill more accurate information of the underlying signals with larger SNRs to signals with lower SNRs. This approach has been demonstrated for classification, regression and denoising of GW signals [13–18, 20]. Specifically, each waveform is normalized to have maximum amplitude 1, and then we use curriculum learning with the decreasing SNR scheme detailed in Table III. The noisy data is then normalized to have variance one. We normalize the data to ensure that the trained model can characterize true BBH signals in realistic detection scenarios, covering a broad range of SNRs.

The different steps followed in our curriculum learning scheme are presented in Table III. In addition, we use an early stopping criterion with the relative error threshold 0.026 for (m_1, m_2) and 0.0016 for $(a_f, \omega_R, \omega_I)$. One additional change to the mass model is we rescale the masses by 1/20, to make the optimization converge faster. In the evaluation, we just scale the data back to its original amplitude.

III. EXPERIMENTAL RESULTS

Using the signal manifold described in the previous section, we present results of the accuracy with which our neural network models can measure the masses of the binary components, and the properties of the corresponding remnant.

Figure 3 presents the accuracy with which (m_1, m_2) can be recovered over a a broad range of SNRs. We notice that for signals with SNR ≥ 15 , the primary and secondary masses can be constrained with relative errors [45] less than (7%, 12%), respectively. These results represent a major improvement to the analysis we reported in the context of a 2-D signal manifold in [13, 14]. Furthermore, Figure 4 shows that for signals with SNR ≥ 15 our neural

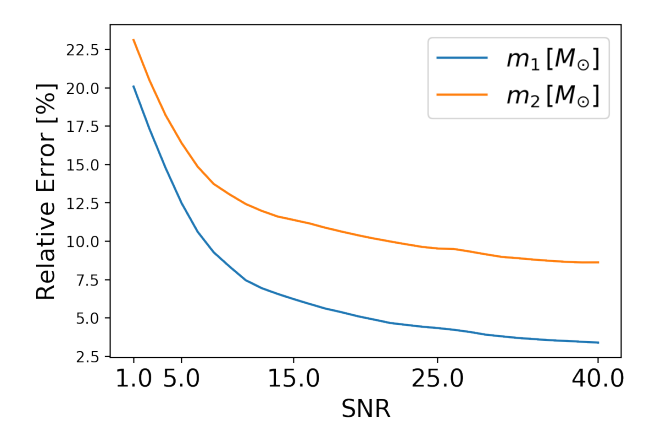


FIG. 3. Relative error with which our deep learning algorithm can measure the masses of the binary black hole components as a function of optimal matched-filtering signal-to-noise ration (SNR). For waveform with SNR \geq 15, the primary and secondary masses can be constrained with relative errors less than (7%, 12%), respectively.

network models can measure the triplet $(a_f, \omega_R, \omega_I)$ with relative errors less than (13%, 5%, 3%), respectively. To the best of our knowledge, this is the first time deep learning is used to infer the properties of BH remnants directly from GW signals.

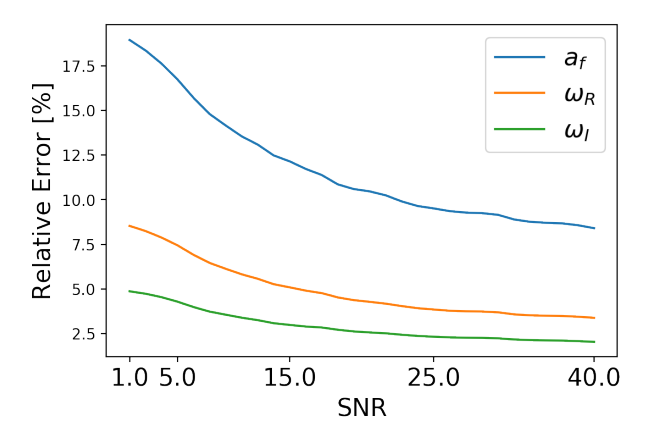


FIG. 4. Relative error, as a function of optimal matchedfiltering signal-to-noise ration (SNR), with which our neural network model can measure the final spin, a_f , and quasinormal modes (QNMs), (ω_R, ω_I) , of the black hole remnant. For signals with SNR ≥ 15 , $(a_f, \omega_R, \omega_I)$ can be recovered with relative errors less than (13%, 5%, 3%), respectively.

IV. DEEP LEARNING PARAMETER ESTIMATION OF DETECTED BINARY BLACK HOLE MERGERS

In this section we use our neural network models to measure $(m_1, m_2, a_f, \omega_R, \omega_I)$ from all the BBH mergers detected to date by the advanced LIGO and Virgo observatories [6]. The results of this analysis are presented

TABLE IV. Deep learning parameter estimation results for the catalog of BBH signals reported in [6]. The values for each parameter, from left to right, represent the median, median absolute deviation and Pearson median skewness, obtained by whitening the GW strain containing a putative signal with up to 120 different PSDs.

		$m_2[{ m M}_{\odot}]$			=
GW150914	37.46 [4.13 0.06]	30.80 [0.43 -1.65]	0.689 [0.037 0.17]	$0.5362 \ [0.0127 -0.20]$	0.0798 [0.0011 0.16]
GW151012	23.89 [0.35] 1.65]	17.34 [0.56 1.44]	0.653 [0.009 0.25]	0.5214 [0.0030 0.15]	0.0810 [0.0003 -0.15]
GW151226	17.60 [2.01] 0.87]	14.14 [2.85] 0.73]	0.646 [0.006 1.53]	0.5188 [0.0021] 1.51]	0.0812 [0.0001 - 1.60]
GW170104	36.45 [1.54]-0.76]	21.83 [3.54]-0.56]	0.661 [0.080]-0.84]	0.5185 [0.0306] - 0.48	0.0816 [0.0029] [0.57]
GW170608	13.96 [1.13] 1.10]	11.96 [1.07] 1.56]	0.697 [0.025 -1.28]	$0.5278 \ [0.0154 -0.95]$	0.0809 [0.0011 -0.67]
GW170729	48.61 [1.58]-1.61]	37.69 [1.82]-0.28]	0.694 [0.019 - 0.47]	0.5102 [0.0107 -0.50]	0.0812 [0.0019]-0.16]
GW170809	31.01 [3.29] 0.60]	22.42 [4.56] 1.85]	0.698 [0.034]-1.23]	0.5428 [0.0163]-1.15]	0.0779 [0.0016]-1.05]
GW170814	35.07 [1.75] 0.84]	21.50 [0.52] 0.99]	0.718 [0.010]-1.89]	0.5377 [0.0108 - 1.38]	0.0794 [0.0003] 1.76]
GW170818	40.05 [1.29]-1.57]	24.08 [0.93]-1.33]	0.656 [0.015] 0.73	0.5129 [0.0043 1.21]	0.0816 [0.0005]-1.02]
GW170823	39.56 [1.75 - 1.44]	30.14 [0.53 -1.68]	0.740 [0.002 -1.76]	0.5510 [0.0007 -1.74]	0.0782 [0.0001 1.75]

in Table IV in triplets that provide, from left to right, the median, median absolute deviation and Pearson median skewness. These values are computed by whitening the data containing a putative signal with 120 different PSDs, half of them are constructed using LIGO Hanford noise and the rest with LIGO Livingstone noise. Through this approach we are effectively measuring the impact of PSD variations in the measurements of the astrophysical parameters of BBH mergers.

The deep learning parameter estimation results presented in Tables IV are consistent with those obtained with established, Bayesian parameter estimation pipelines [6]. The robustness and speed with which these results are obtained for each BBH signal (less than 2 milliseconds) warrants the development in full generality of the algorithms we present in this article. This work is under earnest development and will be presented shortly.

Having demonstrated the application of deep learning at scale for the characterization of BBH mergers, it is now in order to design deep neural networks for realtime detection and characterization of GW sources that are expected to have electromagnetic and astro-particle counterparts, i.e., BNS and NSBH systems. For that study, we expect no additional computational challenges to the ones we have already addressed in this analysis. The central development for such an effort, however, will consist of designing a clever algorithm to readily identify BNS or NSBH in a hierarchical manner, i.e., in principle it is not needed to train neural networks using minute long waveforms. Rather, we need to figure out how much information is needed to accurately reconstruct the astrophysical parameters of one of these events in real-time. These studies should be pursued in the future.

V. CONCLUSION

We have presented the first application of deep learning at scale to characterize the astrophysical properties of BHs whose spins are aligned or anti-aligned, and which evolve on quasi-circular orbits. Using nearly 10 mil-

lion waveforms to densely sample this parameter space, and encoding time- and scale-invariance, we have demonstrated that deep learning enables real-time GW parameter estimation. Our results are consistent with established, compute-intensive, Bayesian methods that are routinely used for GW parameter estimation.

The approach we have presented herein provides the means to constrain the parameters of BBHs before and after the merger event. We have shown that deep learning can directly infer the final spin and QNMs of BH remnants, thereby paving the way to directly use QNMs to assess whether BH remnants are accurately described by general relativity. In future work, we will study how accurately these neural network models can tell apart ringdown waveforms described by astrophysically motivated alternative theories of gravity in realistic detection scenarios. The extension of this work to enable real-time detection and parameter estimation of GW sources that are central for Multi-Messenger Astrophysics discovery campaigns should also be investigated.

VI. ACKNOWLEDGEMENTS

This research is part of the Blue Waters sustainedpetascale computing project, which is supported by the National Science Foundation (awards OCI-0725070 and ACI-1238993) and the State of Illinois. Blue Waters is a joint effort of the University of Illinois at Urbana-Champaign and its National Center for Supercomputing Applications. We acknowledge support from the NCSA, and thank the NCSA Gravity Group for useful feedback. Tesla P100 and V100 GPUs used for this project were donated by NVIDIA to the NCSA Gravity Group, and are hosted by Vlad Kindratenko at the Innovative Systems Lab at NCSA. This work also made used the Extreme Science and Engineering Discovery Environment (XSEDE), which is supported by National Science Foundation grant number ACI-1548562. Specifically, it used the Bridges system, which is supported by NSF award number ACI-1445606, at the Pittsburgh Supercomputing Center (PSC); TG-PHY160053 grant is gratefully acknowledged This research used resources of the Argonne Leadership Computing Facility, which is a DOE

Office of Science User Facility supported under Contract DE-AC02-06CH11357. This paper was reviewed and approved by the LIGO P&P committee.

- [1] B. P. Abbott, R. Abbott, T. D. Abbott, M. R. Abernathy, F. Acernese, K. Ackley, C. Adams, T. Adams, P. Addesso, R. X. Adhikari, and et al., Physical Review Letters 116, 061102 (2016), arXiv:1602.03837 [gr-qc].
- [2] B. P. Abbott, R. Abbott, T. D. Abbott, M. R. Abernathy, F. Acernese, K. Ackley, C. Adams, T. Adams, P. Addesso, R. X. Adhikari, and et al., Physical Review Letters 116, 241103 (2016), arXiv:1606.04855 [gr-qc].
- [3] B. P. Abbott, R. Abbott, T. D. Abbott, M. R. Abernathy, F. Acernese, K. Ackley, C. Adams, T. Adams, P. Addesso, R. X. Adhikari, et al., Physical Review Letters 118, 221101 (2017).
- [4] B. P. Abbott, R. Abbott, T. D. Abbott, F. Acernese, K. Ackley, C. Adams, T. Adams, P. Addesso, R. X. Adhikari, V. B. Adya, and et al., Physical Review Letters 119, 141101 (2017), arXiv:1709.09660 [gr-qc].
- [5] B. P. Abbott, R. Abbott, T. D. Abbott, F. Acernese, K. Ackley, C. Adams, T. Adams, P. Addesso, R. X. Adhikari, V. B. Adya, and et al., Astrophys. J. Lett 851, L35 (2017), arXiv:1711.05578 [astro-ph.HE].
- [6] The LIGO Scientific Collaboration, the Virgo Collaboration, et al., arXiv e-prints, arXiv:1811.12907 (2018), arXiv:1811.12907 [astro-ph.HE].
- [7] B. P. Abbott, R. Abbott, T. D. Abbott, M. R. Abernathy, F. Acernese, K. Ackley, C. Adams, T. Adams, P. Addesso, R. X. Adhikari, and et al., Physical Review Letters 116, 131103 (2016), arXiv:1602.03838 [gr-qc].
- [8] The LIGO Scientific Collaboration, J. Aasi, et al., Classical and Quantum Gravity 32, 074001 (2015), arXiv:1411.4547 [gr-qc].
- [9] F. Acernese et al., Classical and Quantum Gravity 32, 024001 (2015), arXiv:1408.3978 [gr-qc].
- [10] LSST Science Collaboration, P. A. Abell, J. Allison, S. F. Anderson, J. R. Andrew, J. R. P. Angel, L. Armus, D. Arnett, S. J. Asztalos, T. S. Axelrod, and et al., ArXiv e-prints (2009), arXiv:0912.0201 [astro-ph.IM].
- [11] G. Allen, W. Anderson, E. Blaufuss, J. S. Bloom, P. Brady, S. Burke-Spolaor, S. B. Cenko, A. Connolly, P. Couvares, D. Fox, A. Gal-Yam, S. Gezari, A. Goodman, D. Grant, P. Groot, J. Guillochon, C. Hanna, D. W. Hogg, K. Holley-Bockelmann, D. A. Howell, D. Kaplan, E. Katsavounidis, M. Kowalski, L. Lehner, D. Muthukrishna, G. Narayan, J. E. G. Peek, A. Saha, P. Shawhan, and I. Taboada, arXiv e-prints, arXiv:1807.04780 (2018), arXiv:1807.04780 [astro-ph.IM].
- [12] G. Allen, I. Andreoni, E. Bachelet, G. B. Berriman, F. B. Bianco, R. Biswas, M. Carrasco Kind, K. Chard, M. Cho, P. S. Cowperthwaite, Z. B. Etienne, D. George, T. Gibbs, M. Graham, W. Gropp, A. Gupta, R. Haas, E. A. Huerta, E. Jennings, D. S. Katz, A. Khan, V. Kindratenko, W. T. C. Kramer, X. Liu, A. Mahabal, K. McHenry, J. M. Miller, M. S. Neubauer, S. Oberlin, J. Olivas, Alexander R., S. Rosofsky, M. Ruiz, A. Saxton, B. Schutz, A. Schwing, E. Seidel, S. L. Shapiro, H. Shen, Y. Shen, B. M. Sipőcz, L. Sun, J. Towns, A. Tsokaros, W. Wei, J. Wells, T. J. Williams, J. Xiong,

- and Z. Zhao, arXiv e-prints, arXiv:1902.00522 (2019), arXiv:1902.00522 [astro-ph.IM].
- [13] D. George and E. A. Huerta, Phys. Rev. D 97, 044039 (2018), arXiv:1701.00008 [astro-ph.IM].
- [14] D. George and E. A. Huerta, Physics Letters B 778, 64 (2018), arXiv:1711.03121 [gr-qc].
- [15] A. Rebei, E. A. Huerta, S. Wang, S. Habib, R. Haas, D. Johnson, and D. George, arXiv e-prints, arXiv:1807.09787 (2018), arXiv:1807.09787 [gr-qc].
- [16] D. George, H. Shen, and E. A. Huerta, ArXiv e-prints (2017), arXiv:1711.07468 [astro-ph.IM].
- [17] D. George and E. A. Huerta, ArXiv e-prints (2017), arXiv:1711.07966 [gr-qc].
- [18] H. Shen, D. George, E. A. Huerta, and Z. Zhao, ArXiv e-prints (2017), arXiv:1711.09919 [gr-qc].
- [19] E. A. Huerta, D. George, Z. Zhao, and G. Allen, arXiv e-prints, arXiv:1805.02716 (2018), arXiv:1805.02716 [cs.LG].
- [20] W. Wei and E. A. Huerta, arXiv e-prints arXiv:1901.00869 (2019), arXiv:1901.00869 [gr-qc].
- [21] A. J. K. Chua, C. R. Galley, and M. Vallisneri, ArXiv e-prints (2018), arXiv:1811.05491 [astro-ph.IM].
- [22] H. Gabbard, M. Williams, F. Hayes, and C. Messenger, Physical Review Letters 120, 141103 (2018), arXiv:1712.06041 [astro-ph.IM].
- [23] X. Fan, J. Li, X. Li, Y. Zhong, and J. Cao, ArXiv eprints (2018), arXiv:1811.01380 [astro-ph.IM].
- [24] J. A. González and F. S. Guzmán, Phys. Rev. D 97, 063001 (2018), arXiv:1803.06060 [astro-ph.HE].
- [25] Y. Fujimoto, K. Fukushima, and K. Murase, *Phys. Rev.* D 98, 023019 (2018), arXiv:1711.06748 [nucl-th].
- [26] X. Li, W. Yu, and X. Fan, ArXiv e-prints (2017), arXiv:1712.00356 [astro-ph.IM].
- [27] H. Nakano et al., ArXiv e-prints (2018), arXiv:1811.06443 [gr-qc].
- [28] P. Graff, F. Feroz, M. P. Hobson, and A. Lasenby, MN-RAS 421, 169 (2012), arXiv:1110.2997 [astro-ph.IM].
- [29] J. Veitch, V. Raymond, B. Farr, W. Farr, P. Graff, S. Vitale, B. Aylott, K. Blackburn, N. Christensen, M. Coughlin, W. Del Pozzo, F. Feroz, J. Gair, C.-J. Haster, V. Kalogera, T. Littenberg, I. Mandel, R. O'Shaughnessy, M. Pitkin, C. Rodriguez, C. Röver, T. Sidery, R. Smith, M. Van Der Sluys, A. Vecchio, W. Vousden, and L. Wade, *Phys. Rev.* D 91, 042003 (2015), arXiv:1409.7215 [gr-qc].
- [30] M. Abadi, P. Barham, J. Chen, Z. Chen, A. Davis, J. Dean, M. Devin, S. Ghemawat, G. Irving, M. Isard, et al., in 12th {USENIX} Symposium on Operating Systems Design and Implementation ({OSDI} 16) (2016) pp. 265–283.
- [31] M. Abadi, A. Agarwal, P. Barham, E. Brevdo, Z. Chen, C. Citro, G. S. Corrado, A. Davis, J. Dean, M. Devin, et al., Software available from tensorflow. org 1 (2015).
- [32] E. Berti, V. Cardoso, and C. M. Will, Phys. Rev. D 73, 064030 (2006), arXiv:gr-qc/0512160.

- [33] J. Healy and C. O. Lousto, Phys. Rev. D 95, 024037 (2017), arXiv:1610.09713 [gr-qc].
- [34] K. Sairam, J. Mukherjee, A. Patra, and P. P. Das, CoRR (2018).
- [35] J. Hu, L. Shen, and G. Sun, in Proceedings of the IEEE conference on computer vision and pattern recognition (2018) pp. 7132–7141.
- [36] X. Dong, G. Kang, K. Zhan, and Y. Yang, CoRR (2017), arXiv:1709.07634.
- [37] R. K. Srivastava, K. Greff, and J. Schmidhuber, arXiv e-prints , arXiv:1505.00387 (2015), arXiv:1505.00387 [cs.LG].
- [38] K. He, X. Zhang, S. Ren, and J. Sun, in *Proceedings* of the IEEE conference on computer vision and pattern recognition (2016) pp. 770–778.
- [39] N. Srivastava, G. Hinton, A. Krizhevsky, I. Sutskever, and R. Salakhutdinov, Journal of Machine Learning Research 15, 1929 (2014).
- [40] J. Blackman, S. E. Field, C. R. Galley, B. Szilágyi, M. A. Scheel, M. Tiglio, and D. A. Hemberger, Physical Review

- Letters 115, 121102 (2015), arXiv:1502.07758 [gr-qc].
- [41] F. Hofmann, E. Barausse, and L. Rezzolla, Astrophys. J. 825, L19 (2016), arXiv:1605.01938 [gr-qc].
- [42] LIGO Lab, the LIGO Scientific Collaboration and the Virgo Scientific Collaboration, "Gravitational wave open science center," (2019), https://www.gw-openscience.org/about/.
- [43] D. P. Kingma and J. Ba, CoRR abs/1412.6980 (2014).
- [44] Y. Bengio, J. Louradour, R. Collobert, and J. Weston, in Proceedings of the 26th Annual International Conference on Machine Learning, ICML '09 (ACM, New York, NY, USA, 2009) pp. 41–48.
- [45] M. Abramowitz and I. A. Stegun, Dover Books on Advanced Mathematics, New York: Dover, —c1965, Corrected edition, edited by Abramowitz, Milton; Stegun, Irene A. (1965).